

SCIENTIFIC REPORTS



OPEN

Quantum gates by periodic driving

Z. C. Shi^{1,2}, W. Wang¹ & X. X. Yi¹

Topological quantum computation has been extensively studied in the past decades due to its robustness against decoherence. One way to realize the topological quantum computation is by adiabatic evolutions—it requires relatively long time to complete a gate, so the speed of quantum computation slows down. In this work, we present a method to realize single qubit quantum gates by periodic driving. Compared to adiabatic evolution, the single qubit gates can be realized at a fixed time much shorter than that by adiabatic evolution. The driving fields can be sinusoidal or square-well field. With the sinusoidal driving field, we derive an expression for the total operation time in the high-frequency limit, and an exact analytical expression for the evolution operator without any approximations is given for the square well driving. This study suggests that the period driving could provide us with a new direction in regulations of the operation time in topological quantum computation.

As a promising avenue to deal with decoherence, topological quantum computations^{1–8} employ two-dimensional quasiparticles called anyons, whose world lines cross over one another to form braids in a three-dimensional spacetime. Information encoded in the anyons is robust against local perturbations, due to the topological nature of anyons, and braiding operation² can be exploited to construct fault-tolerant quantum computation⁹. Majorana fermions, the simplest example of non-Abelian anyons, are predicted to exist in fractional quantum Hall systems¹⁰, topological insulators^{11,12}, solid state systems¹³, and semiconductor-superconductor hybrid systems^{14–16}. More recently, the signatures of Majorana fermions have also been observed in experiments^{17–21}, which gives rise to an opportunity to encode a qubit by Majorana fermions in these materials.

The adiabatic evolution has been widely applied to preparation and manipulation of Majorana fermions^{22–25}. In particular, it has been shown that topological quantum information processing becomes possible in the one-dimensional network²⁵ by adiabatically controlling the locally tunable gates which affect the chemical potential over a finite length of the topological superconductor (TS) wire. The main idea of adiabatic computation is that, design a Hamiltonian H_1 whose ground state is the target state $|\psi_T\rangle$ while the ground state $|\psi_0\rangle$ of Hamiltonian H_0 is easily to be prepared. Assume that there exists a quantum system described by the following Hamiltonian,

$$H = \left[1 - f\left(\frac{t}{T}\right) \right] H_0 + f\left(\frac{t}{T}\right) H_1, \quad (1)$$

where $f(t)$ is a slowly varying function of time t with $f(0) = 0$ and $f(1) = 1$. According to the adiabatic theorem, the quantum system evolves adiabatically from the initial (ground) state $|\psi_0\rangle$ to the target (ground) state $|\psi_T\rangle$ at time $t = T$, solving the problem associated with the target state $|\psi_T\rangle$. The price one shall pay in adiabatic computation is the long evolution time required by adiabatic condition.

Since a quantum task is often accomplished by a sequence of quantum operations rather than a single quantum operation^{23–29}, the total operation time increases linearly with the number of quantum operations. On the other hand, with respect to the limit of the coherence time in quantum systems, long operation time is not favorable for quantum computation, even for topological quantum computation which is robust against perturbations. Hence it is not suitable for implementing quantum operations by adiabatic evolution if the coherence time of quantum systems are short. This gives rise to a question that are there any other methods to achieve the goals better than adiabatic passage?

The time-periodic driving systems have been extensively studied in the past few years. Several work^{30–41} have shown that topological properties of system can be changed by time-periodic driving (e.g., the existence of Floquet topological insulators or Floquet Majorana fermions). Recently, the Floquet Majorana fermions are realized by periodic driving fields in the system of coupled quantum dots proximity to a s -wave superconductor⁴².

¹Center for Quantum Sciences and School of Physics, Northeast Normal University, Changchun 130024, China.

²School of Physics and Optoelectronic Technology Dalian University of Technology, Dalian 116024, China. Correspondence and requests for materials should be addressed to X.X.Y. (email: yixx@nenu.edu.cn)

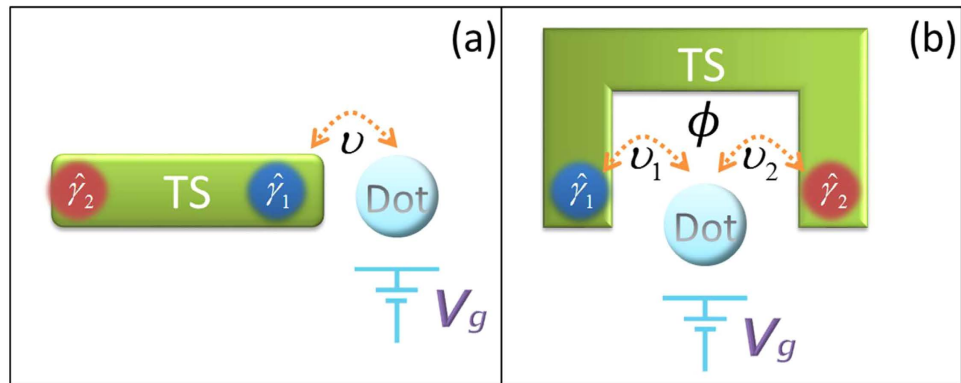


Figure 1. The schematic setup for realizing the operation P_1 .

More recently, it has been proposed to achieve the direct coupling between the topological and conventional qubits by periodic driving fields⁴³. In this work we explore the possibility to regulate the total operation time by periodic driving. Of course, this method can also be extended to the other quantum systems.

Results

The physical model of interest consists of a quantum dot coupling to a TS nanowire, as shown in Fig. 1(a). In the magnetic field, by proximity coupling to a superconductor, one can prepare Majorana modes in the nanowire with strong spin-orbit interaction in the topological phase^{15,16,44,45}. Then the effective Hamiltonian (in the low-energy limit) for the quantum dot coupling to the Majorana mode reads⁴⁶

$$H = \varepsilon(t)\hat{a}^\dagger\hat{a} + (v^*\hat{a}^\dagger - v\hat{a})\hat{\gamma}_1, \quad (2)$$

where a (a^\dagger) is the annihilation (creation) operator for electron in the quantum dot and the on-site energy $\varepsilon(t)$ of the quantum dot can be controlled by the gate voltage V_g . v denotes the tunnel coupling between the quantum dot and the Majorana mode $\hat{\gamma}_1$. Without loss of generality we assume v is a real number and take all physical parameters in units of v . Since the Majorana mode $\hat{\gamma}_i$ ($i = 1, 2$) is Hermitian ($\hat{\gamma}_i^\dagger = \hat{\gamma}_i$ and $\hat{\gamma}_i^2 = 1$), we cannot use the number operator $\hat{\gamma}_i^\dagger\hat{\gamma}_i$ to count the population of Majorana mode. Nevertheless, two Majorana modes can be combined to generate one ordinary fermion, e.g., $\hat{b} = \frac{\hat{\gamma}_1 + i\hat{\gamma}_2}{2}$. One can adopt the number operator $\hat{b}^\dagger\hat{b}$ of the ordinary fermion to count Majorana modes.

Due to the conservation of total parity, defined by the electron in quantum dot and the ordinary fermion formed by Majorana modes, the Hamiltonian is block diagonal in the basis spanned by $\{|0\rangle_F|0\rangle_D, |1\rangle_F|1\rangle_D, |1\rangle_F|0\rangle_D, |0\rangle_F|1\rangle_D\}$.

$$H = \begin{pmatrix} 0 & v & 0 & 0 \\ v & \varepsilon(t) & 0 & 0 \\ 0 & 0 & 0 & v \\ 0 & 0 & v & \varepsilon(t) \end{pmatrix}. \quad (3)$$

We have used $|m\rangle_F|n\rangle_D$ to describe system state, where m is the number of ordinary fermion formed by the Majorana modes and n is the number of electron in the quantum dot. It has been suggested⁴⁶ that by adiabatically changing the values of the on-site energy $\varepsilon(t)$ from $-\infty$ to $+\infty$, one can realize the operation P_1 which denotes the population inversion in the ordinary fermion formed by the Majorana modes, i.e.,

$$P_1(\sin\theta|0\rangle_F + \cos\theta|1\rangle_F) = \sin\theta|1\rangle_F + \cos\theta|0\rangle_F. \quad (4)$$

Actually, the operation P_1 is equivalent to the action of operator $\hat{\gamma}_1$, i.e., $P_1 = \hat{\gamma}_1$.

We first present the results of realizing the operation P_1 by adiabatic evolution. Figure 2 shows different dynamical behaviors with different changing rates of the on-site energy $\varepsilon(t)$. Note that we employ $V(t)$ defined by $V(t) = \left| \frac{\langle E_1(t) | \dot{E}_2(t) \rangle}{E_1(t) - E_2(t)} \right|$ to quantify the adiabatic condition, where $|E_i(t)\rangle$ ($i = 1, 2$) is the instantaneous eigenstate (the corresponding eigenvalue is denoted by $E_i(t)$) of the Hamiltonian in the even (or odd) subspace. It can be observed in Fig. 2(a) that the operation P_1 cannot be achieved perfectly since the changing rate of the on-site energy $\varepsilon(t)$ is too fast to satisfy the adiabatic condition very well, reflecting in the aspect that $V(t) \ll 1$ cannot be fulfilled all the time. In order to successfully realize the operation P_1 , the changing rate of on-site energy $\varepsilon(t)$ should be slow, which increase the operation time (cf. Fig. 2(c,d)). Considering that the operation P_1 is necessary to implement single qubit rotations or non-Abelian operations, the total operation time would be proportional to the number of operation P_1 .

Besides, noting that the Majorana based qubits may be sensitive to the decoherence induced by electron tunnel coupling to an environment (e.g., leads)^{47–50}, the adiabatic operation may have no use in minimizing the influence

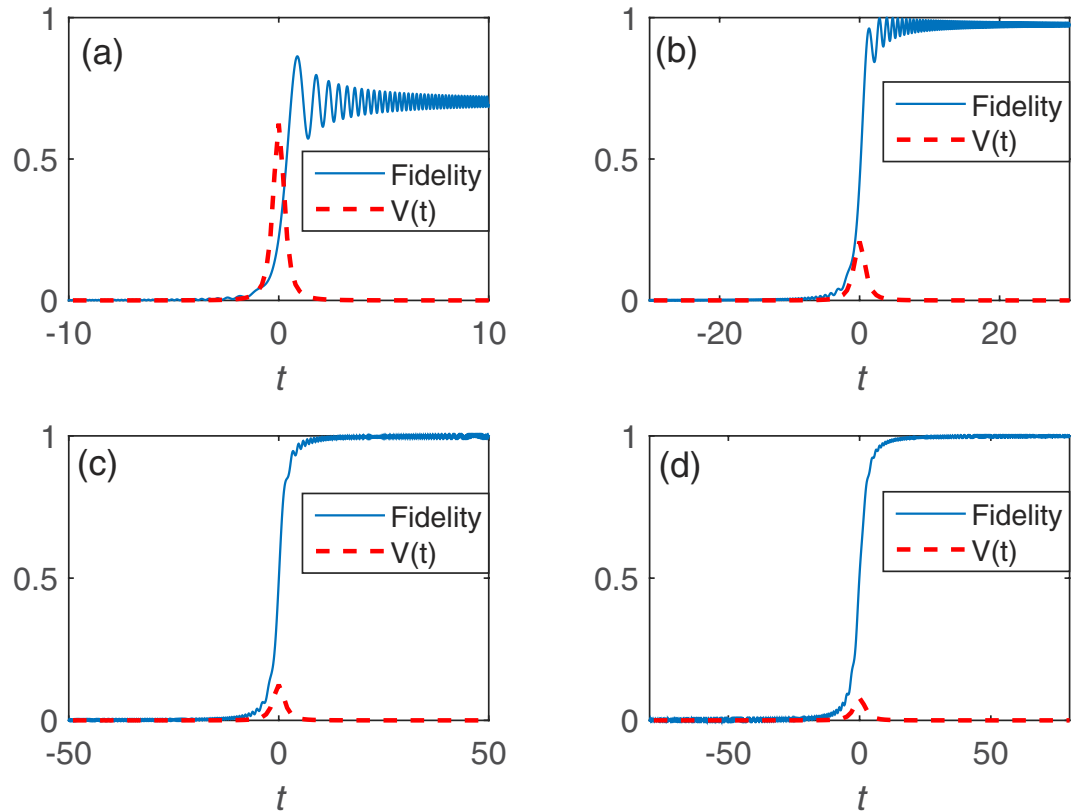


Figure 2. Fidelity and V as a function of time in the realization of the operation P_1 . Here the fidelity is defined as $|\langle \psi(t) | \psi_T \rangle|^2$. The initial state is $|\psi(0)\rangle = \sin \theta |0\rangle_F + \cos \theta |1\rangle_F$ and the target state is $|\psi_T\rangle = \sin \theta |1\rangle_F + \cos \theta |0\rangle_F$, $\theta = \frac{\pi}{6}$. We have set the on-site energy of the quantum dot to increase linearly with time, e.g., $\varepsilon(t) = \frac{50}{T}t$. The operation time is $2T$ and the final value of $\varepsilon(t)$ is 50 during the time evolution. All parameters are in units of the tunnel coupling v . (a) $T = 10$. (b) $T = 30$. (c) $T = 50$. (d) $T = 80$. Large T means small changing rate of the on-site energy $\varepsilon(t)$. One can find that the time to obtain the operation P_1 is about $2T = 100$.

of the decoherence. Recently, the adiabatic evolution can be speeded up by the short-cut scheme and it has been used in the non-Abelian braiding with Y-junction structure⁵¹, but it needs coupling between distinct Majorana modes which seems not very easy in experiment. We will demonstrate in the following that the operation time can be regulated by periodic driving.

Sinusoidal driving. We first consider a periodic modulation of the on-site energy for the quantum dot, where the on-site energy takes the sinusoidal form $\varepsilon(t) = \varepsilon_0 \cos(\omega t)$. The modulation can be generated by waveform generator experimentally and we would also call $\varepsilon(t)$ as driving field hereafter. For a periodic driving system, it is instructive to make definite on the time-scale during evolution. Since the Floquet state $|\phi(t)\rangle$ has the same period with the driving field (see Methods), it affects the system dynamics on short time-scale in the high-frequency limit. What really affects the long time-scale of the system dynamics is the gap of quasi-energies. Therefore, it is helpful to estimate the gap of quasi-energies in the periodic driving system. In order to obtain an approximate expression for quasi-energies, we solve the time-dependent Schrödinger equation by standard perturbation theory, where the tunnel term is regarded as a perturbation. After some algebra, the quasi-energies gap is given by $\Delta = 2 \left| v \mathcal{J}_0 \left(\frac{\varepsilon_0}{\omega} \right) \right|$ (see Methods). Figure 3(a,b) demonstrate the relation between the parameters of driving field and the quasi-energies gap, while Fig. 3(c–e) show the time evolution of the system with different quasi-energies gaps. Obviously, the time-scale of system dynamics gets short with the increasing of the quasi-energies gap. An inspection of Fig. 3(a) also shows that the operation time varies with the decreasing of the amplitude of driving field at a fixed high frequency. Therefore, we can control the operation time in the periodic driving system by properly regulating the frequency and amplitude of driving field. Interestingly, there exists a special case where the quasi-energies vanish at a designated amplitude and frequency of driving field (namely two quasi-energies are degenerate), which is known as the coherent destruction^{52,53}. As a consequence the state is highly localized, and it is not valid to achieve the operation P_1 , as shown in Fig. 3(d).

Taken $|\psi(0)\rangle \simeq \frac{1}{\sqrt{2}}(|\varepsilon_1\rangle - |\varepsilon_2\rangle)$ as the initial state, where $|\varepsilon_1\rangle$ and $|\varepsilon_2\rangle$ are given in Methods, the time evolution of periodic driving system reads

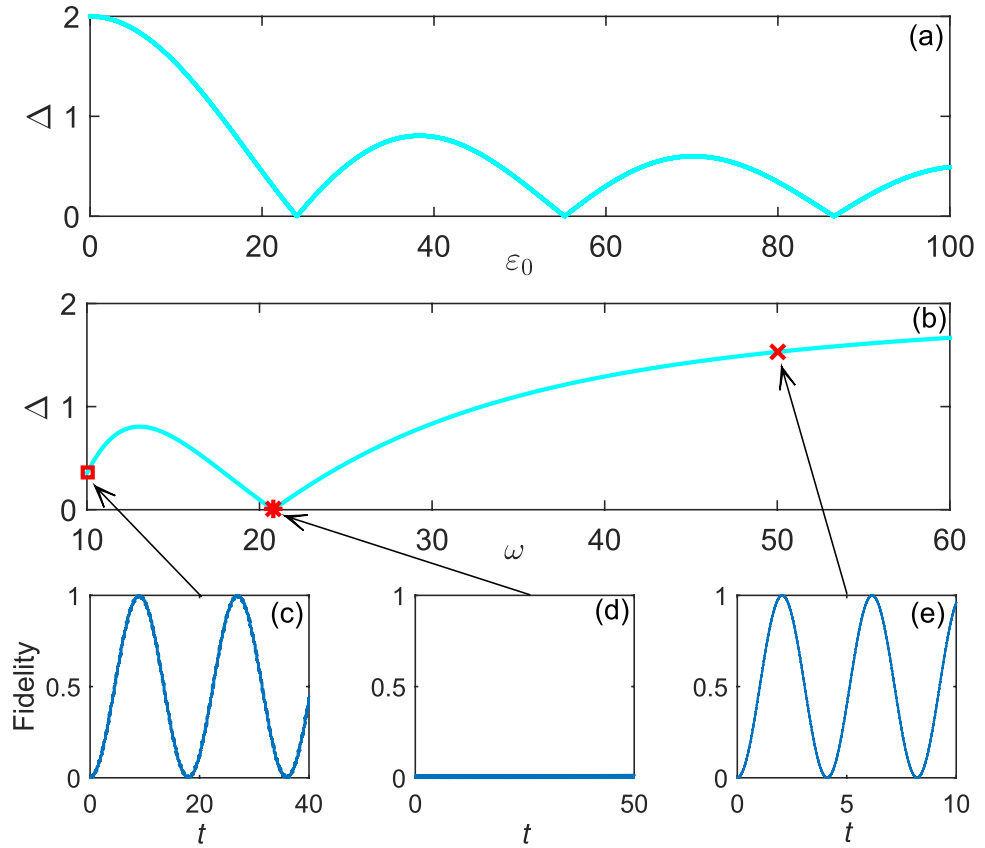


Figure 3. The quasi-energies gap versus (a) the amplitude ε_0 when $\omega = 10$, (b) the frequency ω when $\varepsilon_0 = 50$. The quasi-energies gap approaches 2 when the driving frequency tends to 60 in panel (b). After that the gap increases slowly with the driving frequency. The system dynamics by sinusoidal driving with (c) $\omega = 10$, (d) $\omega = 20.8$, and (e) $\omega = 50$. All parameters are in units of the tunnel coupling v .

$$\begin{aligned}
 |\psi(t)\rangle &\simeq \frac{1}{\sqrt{2}}(e^{-i\varepsilon_1 t}|\varepsilon_1\rangle - e^{-i\varepsilon_2 t}|\varepsilon_2\rangle) \\
 &\simeq \cos\left[\mathcal{J}_0\left(\frac{\varepsilon_0}{\omega}\right)vt\right]|\lambda_2\rangle - i \sin\left[\mathcal{J}_0\left(\frac{\varepsilon_0}{\omega}\right)vt\right]|\lambda_1\rangle.
 \end{aligned}
 \tag{5}$$

We find that the total operation time for realizing the operation P_1 approximately equals

$$\mathcal{T} \simeq \frac{\pi}{2v\left|\mathcal{J}_0\left(\frac{\varepsilon_0}{\omega}\right)\right|}.
 \tag{6}$$

Figure 4 depicts the relation between the total operation time and the amplitude as well as the frequency of the driving field. It suggests that one should avoid the parameter regions where the coherent destruction of tunneling occurs, since it would take a long operation time to realize the operation P_1 if the destruction happens. Outside these parameter regions, the total operation time can be regulated within a range. Besides, one can readily find in Eq. (5) that the fidelity to realize P_1 is

$$F = \sin^2\left[\mathcal{J}_0\left(\frac{\varepsilon_0}{\omega}\right)vt\right] = \frac{1}{2}\left[1 - \cos\left[2\mathcal{J}_0\left(\frac{\varepsilon_0}{\omega}\right)vt\right]\right].
 \tag{7}$$

We plot the coefficients in the fidelity as a function of the quasi-energies gap by exact and perturbative calculations in Fig. 5. It demonstrates that the perturbation results work very well in the high-frequency limit.

In order to check the validity of perturbation theory, we plot the system dynamics with different driving frequencies in Fig. 6. We observe that the dynamics is in excellent agreement with the results by perturbation theory when $\omega > 10$ (in units of v), while it deviates seriously from the perturbation results when $\omega < 10$ (see the pink dot-dash line in Fig. 6). This suggests that the perturbation theory can be safely used when the frequency of the driving field is at least an order of magnitude larger than the tunnel coupling.

Since the perturbation theory is invalid in the low-frequency limit, one might ask how the system behaves in this limit. If the driving frequency is sufficiently small, the adiabatic condition holds in that the on-site energy

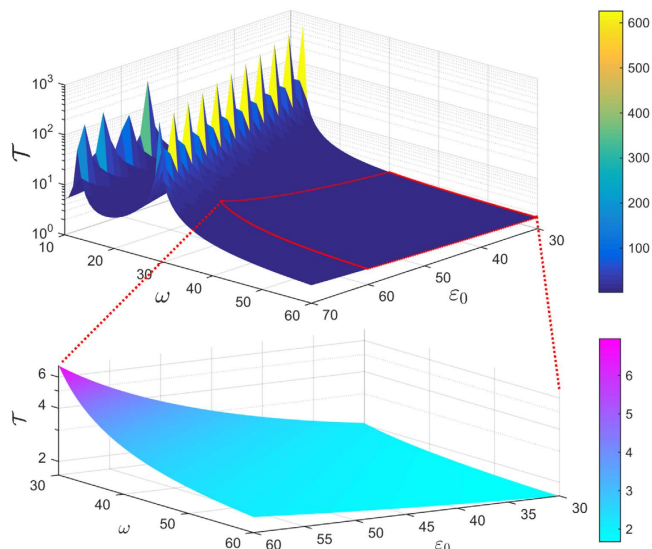


Figure 4. The total operation time \mathcal{T} versus the amplitude ε_0 and the frequency ω of the driving field.

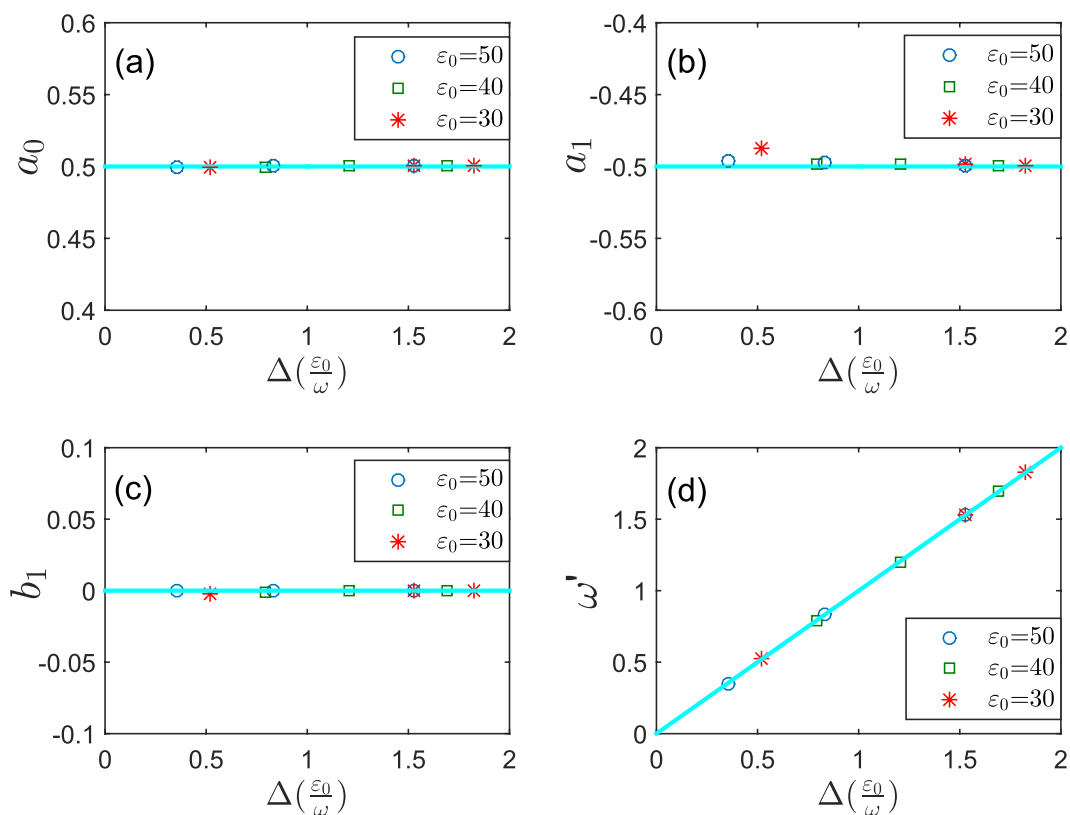


Figure 5. The coefficients (a) a_0 , (b) a_1 , (c) b_1 , and (d) ω' in the fidelity expression versus the quasi-energies gap. The fidelity expression by curve-fitting in MATLAB is given by $F' = a_0 + a_1 \cos \omega' t + b_1 \sin \omega' t$. The lines represent the perturbation results given by Eq. (7), while the circles, squares, and stars represent exact results obtained by curve-fitting. Note that the curve-fitting has high degree of precision for the exact results since the values of *R-square* and *Adjusted R-square* approach 1 ($\geq 99.37\%$) in MATLAB.

changes slowly. We expect that system dynamics (e.g., the fidelity) would manifest periodically at long time-scale (the “period” $T = \frac{2\pi}{\omega}$). Figure 7 demonstrates the evolution with different parameters of the driving field, where the periodic dash lines verifies our expectation. Besides, one can observe in Fig. 7(a) that high fidelity lasts long time within a period when the frequency of driving field is small, and the fidelity dramatically changes when the

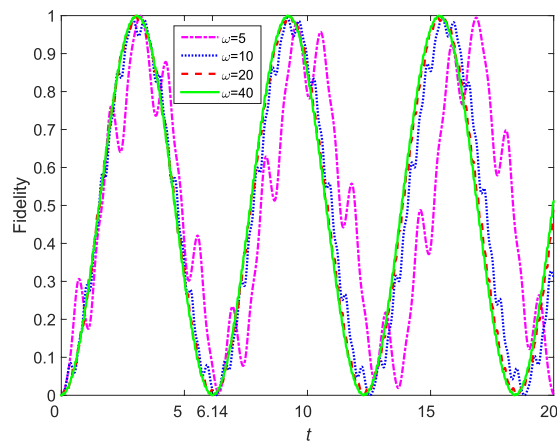


Figure 6. The evolution of fidelity with different frequencies of driving field. We have set the quasi-energies gap $\Delta = 2 \left| \nu \mathcal{J}_0 \left(\frac{\varepsilon_0}{\omega} \right) \right| = 1.0236$, thus the “period” of the system dynamics is about $T \simeq \frac{2\pi}{\Delta} = 6.1383$ in the high-frequency limit, which is confirmed by the green solid line and red dash line in this figure.

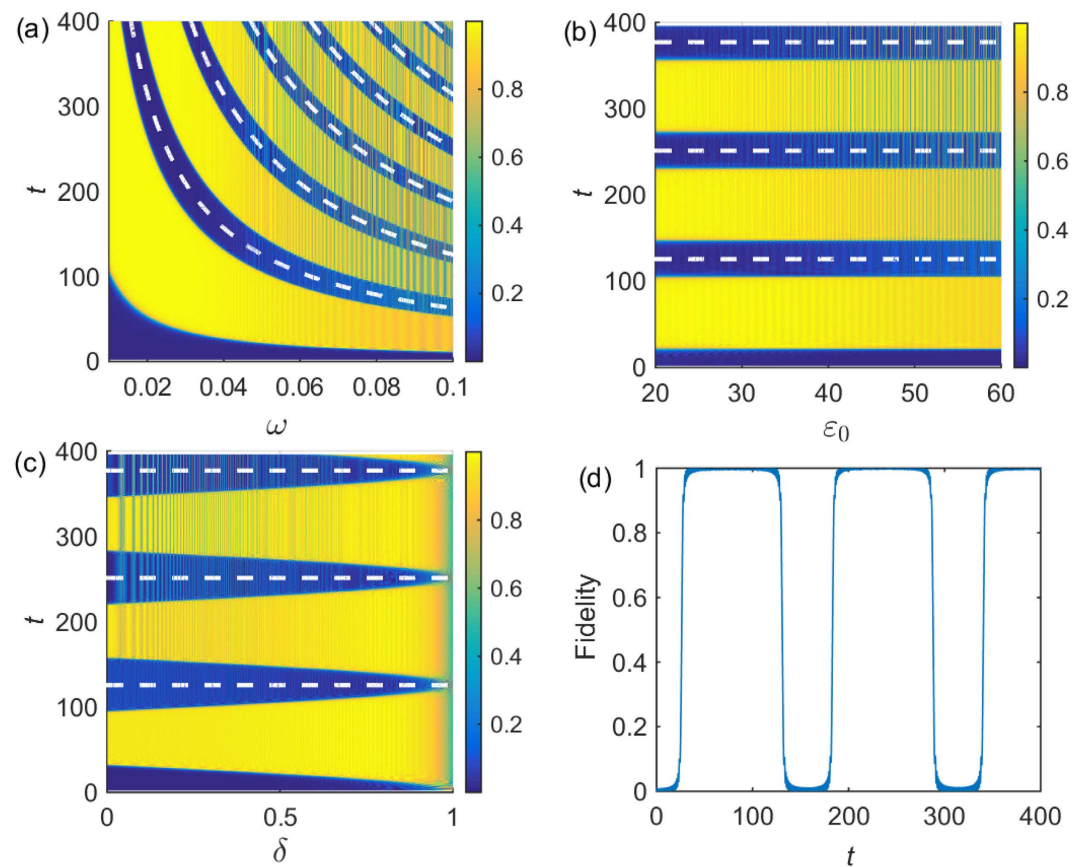


Figure 7. Fidelity as a function of time and different parameters of driving field. The form of driving field takes $\varepsilon(t) = \varepsilon_0 \cos \omega t - \xi$, where ξ is the offset energy of the driving field. (a) $\varepsilon_0 = 40$, $\xi = 20$. (b) $\omega = 0.05$, $\xi = 0.5\varepsilon_0$. (c) $\varepsilon_0 = 40$, $\omega = 0.05$, $\xi = \delta\varepsilon_0$. (d) $\varepsilon_0 = 40$, $\omega = 0.04$, $\xi = 20$. The dash lines are plotted at $t = \frac{2\pi}{\omega}n$, where n is an integer running number.

frequency of driving field is large (i.e., the yellow lines and blue lines alter frequently). The system dynamics becomes considerably complicated when the amplitude of driving field is large, as shown in Fig. 7(b,c) illustrates how the offset energy of quantum dot affects the system dynamics. Interestingly, high fidelity lasts longer time (see the yellow region) when the offset energy of quantum dot is larger. Note that if the offset energy of quantum dot is sufficiently large, e.g., $\xi > \varepsilon_0$, the system dynamics would halt since the value of on-site energy $\varepsilon(t)$ is always

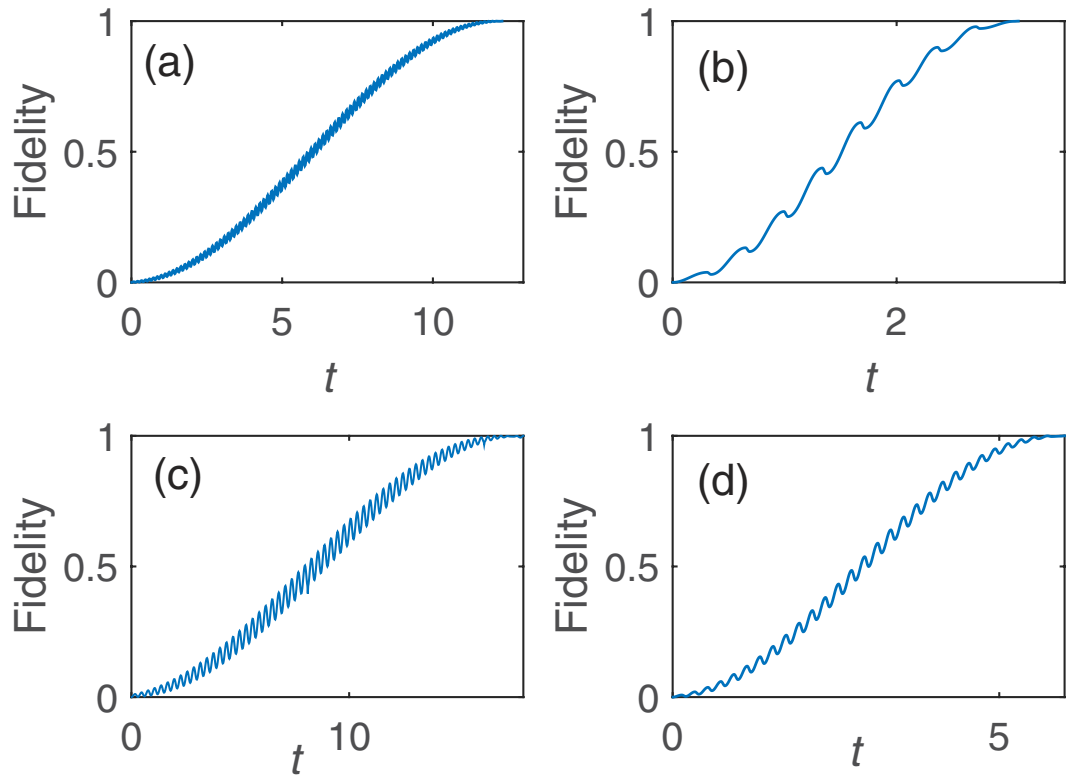


Figure 8. The system dynamics with different forms of square-well driving. (a) $\varepsilon_1 = 40, \varepsilon_2 = 60$. (b) $\varepsilon_1 = 10, \varepsilon_2 = 90$. (c) $T = 0.3, N = 60$. (d) $T = 0.2, N = 30$. The other two parameters are calculated by Eqs (9) and (29).

positive. Figure 7(d) shows the fidelity as a function of time, indicating that the operation time is about 40 and the time with high fidelity lasts about 80.

Square-well driving. The periodic square-well field is another waveform that can be easily achieved in practice. In fact these driving fields have already been studied extensively in time-periodic driving system. Recently, it has been shown in experiment⁵⁴ that the Stückelberg interference occurs in a superconducting qubit driven by square-well field. The square-well driving for the on-site energy of the quantum dot can be expressed as,

$$\varepsilon(t) = \begin{cases} \varepsilon_1, & nT \leq t < t_1 + nT, \\ \varepsilon_2, & t_1 + nT \leq t < (n+1)T, \end{cases} \quad (8)$$

where $n = 1, \dots, N$ and $t_1 \in [0, T]$. T is the period of square-well driving and N is the number of evolution period. To realize the operation P_1 , the form of square-well field should satisfy (see Methods)

$$T = t_1 + t_2, \quad t_1 = \frac{\pi}{\sqrt{4v^2 + \varepsilon_1^2}}, \quad t_2 = \frac{\pi}{\sqrt{4v^2 + \varepsilon_2^2}},$$

$$N = \frac{\pi}{2 \arctan \frac{2v(\varepsilon_2 - \varepsilon_1)}{4v^2 + \varepsilon_1\varepsilon_2}}. \quad (9)$$

According to Eq. (9) the number of evolution period N is not an integer in general. Nevertheless it does not affect the results much because we can take an integer nearest to N (the fidelity increases slowly when it approaches 1). In turn, if one designates the period T and the number of evolution period N of the driving system, the values of on-site energy ε_1 and ε_2 can be resolved by Eq. (9) as well.

Figure 8 show the dynamics of the system with different parameters, where Fig. 8 (a,b) are for different ε_1 and ε_2 while Fig. 8 (c,d) are for different T and N . As expected, P_1 can also be realized in the system driven by a square-well field, and the operation time would be shorter if the difference between ε_1 and ε_2 gets larger.

δ -kick. When the on-site energy $\varepsilon_2 \rightarrow +\infty$, one readily finds in Eq. (9) that $t_2 \rightarrow 0$. Then the square-well field reduces to a periodic δ -kick, i.e.,

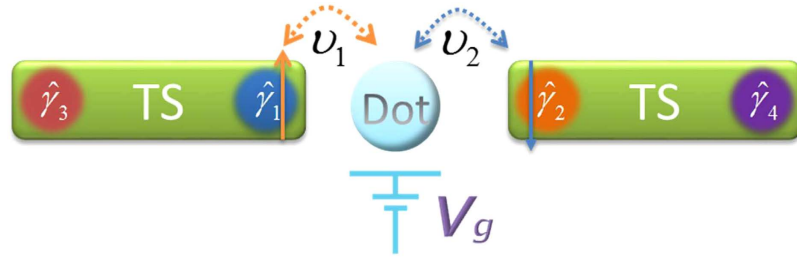


Figure 9. The schematic setup to entangle a conventional qubit and topological qubit.

$$\varepsilon(t) = \varepsilon_1 + \varepsilon_2 \sum_{n=1}^N \delta(t - nT), \tag{10}$$

where T is the period of δ -kick calculated via $T \simeq \frac{\pi}{\sqrt{4v^2 + \varepsilon_1^2}}$. The total operation time for realizing the operation P_1 becomes,

$$T \simeq \frac{\pi^2}{2\sqrt{4v^2 + \varepsilon_1^2} \arctan \frac{2v}{\varepsilon_1}}. \tag{11}$$

Note that the dynamic behavior of system with the δ -kick is quite different from that without it. This can be confirmed by examining a case that the system is under a static driving field ε_1 , where the evolution operator U reads,

$$U(t, 0) = e^{-\frac{i\varepsilon_1 t}{2}} \begin{pmatrix} \cos \frac{xt}{2} + i\frac{\varepsilon_1}{x} \sin \frac{xt}{2} & -i\frac{2v}{x} \sin \frac{xt}{2} \\ -i\frac{2v}{x} \sin \frac{xt}{2} & \cos \frac{xt}{2} - i\frac{\varepsilon_1}{x} \sin \frac{xt}{2} \end{pmatrix}, \quad x = \sqrt{\varepsilon_1^2 + 4v^2}. \tag{12}$$

The fidelity to realize the operation P_1 takes $\left| \frac{2v}{x} \sin \frac{xt}{2} \right|^2$, yielding the maximum of fidelity $\left| \frac{2v}{x} \right|^2$. One easily observes that it cannot obtain the operation P_1 when $\frac{2v}{x} \simeq 0$, i.e., the on-site energy $\varepsilon_1 \gg 1$. However the situation changes in the presence of δ -kick, where the operation P_1 can be achieved regardless of the value of the on-site energy ε_1 (the value of ε_1 determines the driving period and operation time). The advantage in this case is that the system is still in a stationary state when we remove the δ -kick after the operation P_1 is completed.

Application to other systems. Not restricted to the above concrete system, the periodic driving method can be widely applied to the other structure of quantum systems. Here we apply it to a system described by the following Hamiltonian⁵⁶, where two TS nanowires couple to a common quantum dot, as illustrated in Fig. 9,

$$H = \varepsilon(t)(\hat{a}_1^\dagger \hat{a}_1 + \hat{a}_1^\dagger \hat{a}_1) + U \hat{a}_1^\dagger \hat{a}_1 \hat{a}_1^\dagger \hat{a}_1 + (v_1^* \hat{a}_1^\dagger - v_1 \hat{a}_1) \hat{\gamma}_1 + (v_2^* \hat{a}_1^\dagger - v_2 \hat{a}_1) \hat{\gamma}_2. \tag{13}$$

$\varepsilon(t)$ is the on-site energy of the quantum dot. $v_i (i = 1, 2)$ denotes the tunnel coupling between the quantum dot and the Majorana mode $\hat{\gamma}_i$. In particular, the spin-up (labeled as \uparrow) and spin-down (labeled as \downarrow) electrons can only tunnel into the Majorana mode $\hat{\gamma}_1$ and $\hat{\gamma}_2$, respectively. U represents the energy contributed by double occupation on the same quantum dot. When U is sufficiently large, the quantum dot is in the Coulomb block regime where it can only hold one electron.

Since the total parity (the electrons in quantum dot and the ordinary fermions formed by Majorana modes) of the hybrid system is conserved, we restrict ourself in the even-parity subspace spanned by $\{|0\rangle_{F_1} |0\rangle_{F_2} |0\rangle_D, |1\rangle_{F_1} |1\rangle_{F_2} |0\rangle_D, |0\rangle_{F_1} |1\rangle_{F_2} |1\rangle_D, |0\rangle_{F_1} |1\rangle_{F_2} |1\rangle_D, |0\rangle_{F_1} |1\rangle_{F_2} |1\rangle_D, |1\rangle_{F_1} |0\rangle_{F_2} |1\rangle_D, |1\rangle_{F_1} |0\rangle_{F_2} |1\rangle_D, |1\rangle_{F_1} |0\rangle_{F_2} |1\rangle_D\}$, where the subscript $F_i (i = 1, 2)$ represents the ordinary fermions formed by Majorana modes. The Hamiltonian then can be written as,

$$H = \begin{pmatrix} 0 & 0 & 0 & v_2 & v_1 & 0 \\ 0 & 0 & v_1 & 0 & 0 & v_2 \\ 0 & v_1^* & \varepsilon(t) & 0 & 0 & 0 \\ v_2^* & 0 & 0 & \varepsilon(t) & 0 & 0 \\ v_1^* & 0 & 0 & 0 & \varepsilon(t) & 0 \\ 0 & v_2^* & 0 & 0 & 0 & \varepsilon(t) \end{pmatrix}. \tag{14}$$

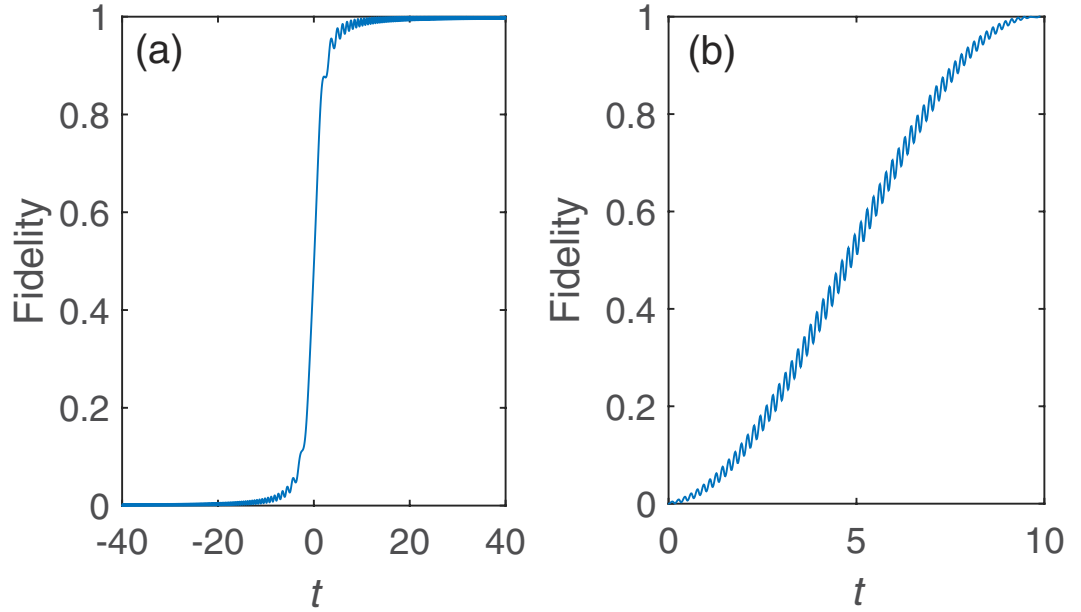


Figure 10. Realizing the operation P_2 by (a) adiabatic evolution and (b) by periodic square-well driving. The on-site energy of quantum dot is $\varepsilon(t) = 1.25t$ in panel (a), and $\varepsilon_1 = 30, \varepsilon_2 = 50$ in panel (b). $\theta = \frac{\pi}{6}$, $v_1 = v_2 = \frac{1}{\sqrt{2}}$. All parameters are in units of v .

This quantum dot-Majorana system^{55,56} can be exploited to prepare entanglement between spin and topological qubits or quantum information transfer between spin and topological qubits (even for quantum logic gates) by adiabatic evolution. We take the preparation of entanglement (denoting as the operation P_2) between the electron spin and Majorana modes as an example to exemplify how to manipulate the operation time by periodic square-well driving given by Eq. (8). The operation P_2 reads,

$$\begin{aligned}
 P_2(\sin \theta |0\rangle_{F_1} |0\rangle_{F_2} + \cos \theta |1\rangle_{F_1} |1\rangle_{F_2}) |0\rangle_D &= \frac{v_1}{v} (\sin \theta |1\rangle_{F_1} |0\rangle_{F_2} + \cos \theta |0\rangle_{F_1} |1\rangle_{F_2}) \\
 &\quad |1\rangle_D \\
 &= + \frac{v_2}{v} (\sin \theta |0\rangle_{F_1} |1\rangle_{F_2} + \cos \theta |1\rangle_{F_1} |0\rangle_{F_2}) \\
 &\quad |1\rangle_D.
 \end{aligned}
 \tag{15}$$

where $v = \sqrt{v_1^2 + v_2^2}$. As the Hamiltonian is a 6×6 matrix, the analytical expression of evolution operator $U(T, 0) = e^{-iH_2 t_2} e^{-iH_1 t_1}$ is involved. Here we only give the equations that determine the period of driving field and the total number of evolution periods, i.e.,

$$\begin{aligned}
 T &= t_1 + t_2, \\
 N &= \frac{\pi}{2 \arctan \frac{x'_4}{x'_3}},
 \end{aligned}
 \tag{16}$$

where $t_1 = \frac{\pi}{\sqrt{\varepsilon_1^2 + 4(v_1^2 + v_2^2)}}$, $t_2 = \frac{\pi}{\sqrt{\varepsilon_2^2 + 4(v_1^2 + v_2^2)}}$, $x'_3 = \varepsilon_1 \varepsilon_2 + 4v_1^2 + 4v_2^2$, and $x'_4 = 2(\varepsilon_2 - \varepsilon_1) \sqrt{v_1^2 + v_2^2}$. Figure 10 plots the fidelity to realize the operation P_2 as a function of time by adiabatic evolution and periodic square-well driving, respectively. Again, the operation time for adiabatic evolution requires relatively long time since it must satisfy adiabatic condition while the operation time and the period can be regulated in square-well driving.

Discussions

Until now, we have studied how to implement the operation P_1 by periodically modulating the on-site energy of the quantum dot. For a single operation P_1 , it is far from sufficient to permit quantum computation. We next briefly discuss how to realize an arbitrary rotation for a Majorana based qubit by successively executing the operation P_1 twice. As shown in Fig. 1(b), the system Hamiltonian reads

$$H = \varepsilon(t) \hat{a}^\dagger \hat{a} + (|v_1| e^{-i\theta_1} \hat{a}^\dagger - |v_1| e^{i\theta_1} \hat{a}) \hat{\gamma}_1 + (|v_2| e^{-i\theta_2} \hat{a}^\dagger - |v_2| e^{i\theta_2} \hat{a}) \hat{\gamma}_2,
 \tag{17}$$

where we have introduced a phase θ_1 (θ_2) into the tunnel coupling v_1 (v_2). Defining the operator $\hat{c} = \hat{a}e^{i\theta_1}$, $z = \sqrt{|v_1|^2 + |v_2|^2}$, $z_1 = \frac{|v_1|}{z}$, and $z_2 = \frac{|v_2|}{z}$, the Hamiltonian (17) becomes,

$$H = \varepsilon(t)\hat{c}^\dagger\hat{c} + z(\hat{c}^\dagger - \hat{c})(z_1\hat{\gamma}_1 + z_2\hat{\gamma}_2), \quad (18)$$

where the phase difference $\theta_1 - \theta_2$ (it can be modulated by the magnetic flux ϕ) equals $2n\pi$, $n = 1, 2, \dots$. The form of Eq. (18) is the same as Eq. (2) if we redefine a new Majorana mode $\hat{\gamma}_{12} = z_1\hat{\gamma}_1 + z_2\hat{\gamma}_2$, where the tunnel coupling is denoted by z . Clearly, the operation $P_1 = \hat{\gamma}_{12}$ in this notation. For a two level system spanned by $\{|0\rangle_{F_1}, |1\rangle_{F_1}\}$, we can express the Majorana operators in terms of Pauli matrices $\{\sigma_x, \sigma_y, \sigma_z\}$, i.e., $\hat{\gamma}_1 = \sigma_x$, $\hat{\gamma}_2 = \sigma_y$, $\hat{\gamma}_1\hat{\gamma}_2 = i\sigma_z$. By successively executing the operation P_1 twice with different relative tunnel strengths, the total operation becomes $P = \hat{\gamma}_{12}\hat{\gamma}'_{12} = (z_1\hat{\gamma}_1 + z_2\hat{\gamma}_2)(z'_1\hat{\gamma}_1 + z'_2\hat{\gamma}_2) = (z_1z'_1 + z_2z'_2) + i(z_1z'_2 - z'_1z_2)\sigma_z$, which is exactly an arbitrary rotation around the z -axis.

Due to the conservation of total parity, a qubit shall be encoded by four Majorana modes⁵⁷. The Majorana based qubit can be realized by the extended model in Fig. 1(b), where the system consists of three quantum dots coupling to four Majorana modes ($\hat{\gamma}_1, \hat{\gamma}_2, \hat{\gamma}_3, \hat{\gamma}_4$) in the TS nanowire with comb structure. In the even-parity subspace spanned by $\{|0\rangle_{F_1}|0\rangle_{F_2}, |1\rangle_{F_1}|1\rangle_{F_2}\}$, the operation $P = \hat{\gamma}_{12}\hat{\gamma}'_{12}$ is in fact the rotation around the z -axis, and the operation $P = \hat{\gamma}_{23}\hat{\gamma}'_{23}$ is the rotation around the x -axis ($\hat{\gamma}_{23} = z_2\hat{\gamma}_2 + z_3\hat{\gamma}_3$), where the ordinary fermion F_1 (F_2) is formed by the Majorana modes $\hat{\gamma}_1$ and $\hat{\gamma}_2$ ($\hat{\gamma}_3$ and $\hat{\gamma}_4$).

Finally, we give a brief discussion on the experimental feasibility of our proposal. In order to avoid quasi-particle excitations in the TS nanowire and two electrons occupying the same quantum dot, the superconducting gap and the Coulomb interaction U are required to be much larger than the tunnel strength λ . For most quantum dot setups the Coulomb interaction U can arrive at the order of meV. Recent experiments^{17,18,58,59} shows that it is sufficient to make the superconducting gap in the order of 0.1–1 meV and the tunnel strength in the order of 1–10 μ eV. Considering electron tunnel from an external environment, the decoherence time of Majorana based qubit is in order of 10 ns–0.1 ms⁴⁹. Besides, due to the electron-phonon interaction the lifetime of quantum dot is in order of 16 ns^{60,61}. When we take the tunnel strength in the order of 1–10 μ eV, the total operation time by periodic driving can reach less than 2 ns, which is much smaller than the system decoherence time. Note that the tunnel coupling between the quantum dot and the Majorana mode depends on both differences among the on-site energies and the tunnel barriers. By making use of periodic driving on the on-site energy of quantum dot, the tunnel coupling would change consequently. Noting that we can employ additional electrostatic gates to manipulate the tunnel barriers, the tunnel coupling can still maintain constant even the on-site energy of quantum dot changes. Indeed, the possibility of controlling the tunnel coupling in semiconductor nanowire has been shown experimentally⁶². So the voltage of electrostatic gates can be manipulated periodically to make the tunnel rate remain unchanged in our system, especially for the periodic square-well case (since it has only two different values of on-site energy).

In summary, we have presented a scheme to realize quantum operation (quantum gates) by periodic driving. The operation time can be exactly controlled by modulating the amplitude or frequency of the driving field. By solving the time-dependent Schrödinger equation with perturbation expansion in the high-frequency limit, we have given an expression for the quasi-energies gap in the sinusoidal driving and found that the total operation time can be manipulated by designing the amplitude and frequency of the driving field. In the low-frequency limit, due to the invalidity of perturbation theory, we study the system dynamics by numerical simulations. The results are almost consistent with those given by adiabatic evolution. Different from adiabatic evolution, the system in the low-frequency limit manifests more intricate behaviors and the operation time can also be regulated by the driving field. In particular, the time that the high fidelity lasts are closely related to the frequency and offset energy of the driving field. With the periodic square-well driving, we have derived an analytical expression for the evolution operator without any approximations. By this expression, we can calculate the amplitude of the square-well driving under fixed operation time and period of the driving field. We have also discussed realization of quantum operations by a δ -kick, which can be treated as a deformed square-well driving. Besides, the periodic driving method can be applied to the other quantum systems—it opens up a new avenue to manipulate the operation time in the topological quantum computation.

Methods

Floquet theory. Assume that the system Hamiltonian is periodic in time, i.e., $H(t) = H(T + t)$, where T is the period and the driving frequency $\omega = \frac{2\pi}{T}$. The Floquet theory⁶³ tells that the solutions of Schrödinger equation have the following form $|\Phi_n(t)\rangle = e^{i\varepsilon_n t}|\phi_n(t)\rangle$, where ε_n is the quasi-energy and the Floquet state $|\phi_n(t)\rangle$ satisfies $|\phi_n(t)\rangle = |\phi_n(T + t)\rangle$. At the same time the eigenvalue equation of the system is ($\hbar = 1$)

$$\left[H(t) - i\frac{\partial}{\partial t} \right] |\phi_n(t)\rangle = \varepsilon_n |\phi_n(t)\rangle, \quad (19)$$

where $H_{\text{eff}} = H(t) - i\frac{\partial}{\partial t}$ is the so-called Floquet operator. To solve this equation it is very instructive to introduce an extended Hilbert space⁶⁴ consisting of time-periodic functions with the inner product defined by $\langle\langle \cdot | \cdot \rangle\rangle = \frac{1}{T} \int_0^T dt \langle \cdot | \cdot \rangle$. We will solve the eigenvalues and eigenstates of the Floquet operator by perturbation theory in the following.

Perturbation theory. With sinusoidal driving, due to the total parity conservation, it is convenient to study in the even parity (or odd parity) subspace. Then the Hamiltonian can be expressed by a 2×2 matrix, which can

be divided into two parts: the on-site energy term $H_\varepsilon(t) = \varepsilon(t)a^\dagger a$ and the tunnel term $H_t = (v^* \hat{a}^\dagger - v \hat{a}) \hat{\gamma}_1$. In this following, we assume that the tunnel term is a perturbation^{65,66}. Since $H_\varepsilon(t) = \varepsilon(t)a^\dagger a$ is diagonal in the space spanned by $\{|0\rangle_F |0\rangle_D, |1\rangle_F |1\rangle_D\}$, when substituting into Eq. (19), the eigenstates of $[H_\varepsilon(t) - i\frac{\partial}{\partial t}]$ are given by

$$\begin{aligned} |\lambda_1(t)\rangle &= (e^{i\lambda_1 t}, 0)^T \\ |\lambda_2(t)\rangle &= (0, e^{i\lambda_2 t - i\frac{\varepsilon_0}{\omega} \sin \omega t})^T, \end{aligned} \tag{20}$$

where λ_i ($i = 1, 2$) is the corresponding eigenvalue (i.e., quasi-energy). In consideration of the periodicity of the Floquet states, two quasi-energies are zero (modulo ω) in the zeroth-order approximation. As a result the two time-dependent eigenstates can be approximately viewed as time-independent eigenstates in the high-frequency limit ($\omega \gg 1$), i.e., $|\lambda_1(t)\rangle = (1, 0)^T$ and $|\lambda_2(t)\rangle \simeq (0, 1)^T$. The quasi-energies in the first-order approximation can be obtained by diagonalizing the matrix⁶⁶

$$\tilde{H}_t = \begin{pmatrix} 0 & Q \\ Q^* & 0 \end{pmatrix}, \tag{21}$$

where the matrix element are calculated by $Q = \frac{v}{T} \int_0^T dt e^{-i\frac{\varepsilon_0}{\omega} \sin \omega t}$. This gives the quasi-energies $\varepsilon_{1,2} = \pm |Q|$ (in the “first Brillouin zone”) and the corresponding eigenstates $|\varepsilon_{1,2}\rangle = \frac{1}{\sqrt{2}}(|\lambda_1(t)\rangle \pm |\lambda_2(t)\rangle)$. The quasi-energies gap is consequently given by $\Delta = 2|Q|$. In the light of the identity

$$e^{i\frac{\varepsilon_0}{\omega} \sin \omega t} = \sum_{n=-\infty}^{\infty} \mathcal{J}_n\left(\frac{\varepsilon_0}{\omega}\right) e^{in\omega t}, \tag{22}$$

where \mathcal{J}_n is the n -order Bessel function, we can finally obtain the analytical expression of quasi-energies gap in the maintext: $\Delta = 2\left|v\mathcal{J}_0\left(\frac{\varepsilon_0}{\omega}\right)\right|$.

The derivation of Eq. (9). With square-well driving, the on-site energy can be written as,

$$\varepsilon(t) = \begin{cases} \varepsilon_1, & nT \leq t < t_1 + nT, \\ \varepsilon_2, & t_1 + nT \leq t < (n + 1)T, \end{cases} \tag{23}$$

where $n = 1, 2, 3 \dots$ and $t_1 \in [0, T]$. The evolution operator U within one period of time takes $U(T, 0) = e^{-iH_2 t_2} e^{-iH_1 t_1}$ with $t_2 = T - t_1$. After some tedious but straightforward algebra, one can obtain,

$$U(T, 0) = \frac{1}{x_1 x_2} e^{-\frac{i}{2}D} \begin{pmatrix} A & B + C \\ B - C & A \end{pmatrix}, \tag{24}$$

where

$$\begin{aligned} A &= -4v^2 \sin \frac{x_1 t_1}{2} \sin \frac{x_2 t_2}{2} + \left(x_1 \cos \frac{x_1 t_1}{2} + i\varepsilon_1 \sin \frac{x_1 t_1}{2}\right) \\ &\quad \times \left(x_2 \cos \frac{x_2 t_2}{2} + i\varepsilon_2 \sin \frac{x_2 t_2}{2}\right) \\ B &= -2iv \left(x_2 \cos \frac{x_2 t_2}{2} \sin \frac{x_1 t_1}{2} + x_1 \cos \frac{x_1 t_1}{2} \sin \frac{x_2 t_2}{2}\right) \\ C &= 2v(\varepsilon_1 - \varepsilon_2) \sin \frac{x_1 t_1}{2} \sin \frac{x_2 t_2}{2}, \\ D &= \varepsilon_1 t_1 + \varepsilon_2 t_2, x_1 = \sqrt{\varepsilon_1^2 + 4v^2}, x_2 = \sqrt{\varepsilon_2^2 + 4v^2}. \end{aligned} \tag{25}$$

At first, we design the driving time t_1 (t_2) for the on-site energy ε_1 (ε_2) to satisfy $x_1 t_1 = \pi$ ($x_2 t_2 = \pi$), that is,

$$t_1 = \frac{\pi}{\sqrt{4v^2 + \varepsilon_1^2}}, t_2 = \frac{\pi}{\sqrt{4v^2 + \varepsilon_2^2}}, t_1 + t_2 = T. \tag{26}$$

Certainly, the period of the square-well driving is fixed. According to Eq. (26), the evolution operator can be further simplified, i.e.,

$$U(T, 0) = \frac{-1}{x_1 x_2} e^{-\frac{i}{2}D} \begin{pmatrix} x_3 & -x_4 \\ x_4 & x_3 \end{pmatrix}, \tag{27}$$

where $x_3 = 4v^2 + \varepsilon_1 \varepsilon_2$ and $x_4 = 2v(\varepsilon_1 - \varepsilon_2)$. After N periods of time, the final evolution operator becomes

$$U(\mathcal{T}, 0) = U(NT, 0) = \frac{1}{2} \left(\frac{-1}{x_1 x_2} \right)^N e^{-\frac{iND}{2}} \cdot \begin{pmatrix} r_1^N + r_2^N & -i(r_1^N - r_2^N) \\ i(r_1^N - r_2^N) & r_1^N + r_2^N \end{pmatrix}, \quad (28)$$

where $r_1 = x_3 - ix_4 = |r|e^{-i\theta}$, $r_2 = x_3 + ix_4 = |r|e^{i\theta}$, $|r| = \sqrt{x_3^2 + x_4^2}$, and $\tan\theta = \frac{x_4}{x_3}$. Clearly, it requires $r_1^N + r_2^N = 0$ in order to realize the operation P_1 perfectly (up to a global phase factor). By making the vectors r_1^N and r_2^N produce a π -phase difference, that is, $N\theta - (-N\theta) = \pi$, one can readily obtain the number of evolution periods,

$$N = \frac{\pi}{2 \arctan \frac{2v(\varepsilon_2 - \varepsilon_1)}{4v^2 + \varepsilon_1 \varepsilon_2}}. \quad (29)$$

References

1. Kitaev, A. Y. Anyons in an exactly solved model and beyond. *Ann. Phys.* **321**, 2–111 (2006).
2. Nayak, C. *et al.* Non-Abelian anyons and topological quantum computation. *Rev. Mod. Phys.* **80**, 1083 (2008).
3. Bonderson, P., Freedman, M. & Nayak, C. Measurement-Only topological quantum computation. *Phys. Rev. Lett.* **101**, 010501 (2008).
4. Miyake, A. Quantum computation on the edge of a symmetry-protected topological order. *Phys. Rev. Lett.* **105**, 040501 (2010).
5. Akhmerov, A. R. Topological quantum computation away from the ground state using Majorana fermions. *Phys. Rev. B* **82**, 020509 (2010).
6. Xue, Z. Y. *et al.* Tunable interfaces for realizing universal quantum computation with topological qubits. *Phys. Rev. A* **88**, 024303 (2013).
7. Mong, R. S. K. *et al.* Universal topological quantum computation from a superconductor-abelian quantum hall heterostructure. *Phys. Rev. X* **4**, 011036 (2014).
8. Wootton, J. R., Burri, J., Iblisdir, S. & Loss, D. Error correction for Non-Abelian topological quantum computation. *Phys. Rev. X* **4**, 011051 (2014).
9. Kitaev, A. Y. Fault-tolerant quantum computation by anyons. *Ann. Phys.* **303**, 2–30 (2003).
10. Read, N. & Green, D. Paired states of fermions in two dimensions with breaking of parity and time-reversal symmetries and the fractional quantum Hall effect. *Phys. Rev. B* **61**, 10267 (2000).
11. Hasan, M. Z. & Kane, C. L. Colloquium: Topological insulators. *Rev. Mod. Phys.* **82**, 3045 (2010).
12. Qi, X. L. & Zhang, S. C. Topological insulators and superconductors. *Rev. Mod. Phys.* **83**, 1057 (2011).
13. Alicea, J. New directions in the pursuit of Majorana fermions in solid state systems. *Rep. Prog. Phys.* **75**, 076501 (2012).
14. Sau, J. D., Lutchyn, R. M., Tewari, S. & Sarma, S. D. Generic new platform for topological quantum computation using semiconductor heterostructures. *Phys. Rev. Lett.* **104**, 040502 (2010).
15. Oreg, Y., Refael, G. & Oppen, F. V. Helical liquids and majorana bound states in quantum wires. *Phys. Rev. Lett.* **105**, 177002 (2010).
16. Lutchyn, R. M., Sau, J. D. & Sarma, S. D. Majorana fermions and a topological phase transition in semiconductor-superconductor heterostructures. *Phys. Rev. Lett.* **105**, 077001 (2010).
17. Das, A. *et al.* Zero-bias peaks and splitting in an Al-InAs nanowire topological superconductor as a signature of Majorana fermions. *Nat. Phys.* **8**, 887–895 (2012).
18. Mourik, V. *et al.* Signatures of Majorana Fermions in Hybrid Superconductor-Semiconductor Nanowire Devices. *Science* **336**, 1003–1007 (2012).
19. Rokhinson, L. P., Liu, X. & Furdyna, J. K. The fractional ac Josephson effect in a semiconductor-superconductor nanowire as a signature of Majorana particles. *Nat. Phys.* **8**, 795 (2012).
20. Perge, S. N. *et al.* Observation of Majorana fermions in ferromagnetic atomic chains on a superconductor. *Science* **346**, 602 (2014).
21. Lee, E. J. H. *et al.* Spin-resolved Andreev levels and parity crossings in hybrid superconductor-semiconductor nanostructures. *Nat. Nanotech.* **9**, 79 (2014).
22. Kraus, C. V., Diehl, S., Zoller, P. & Baranov, M. A. Preparing and probing atomic Majorana fermions and topological order in optical lattices. *New J. Phys.* **14**, 113036 (2012).
23. Clarke, D. J., Sau, J. D. & Tewari, S. Majorana fermion exchange in quasi-one-dimensional networks. *Phys. Rev. B* **84**, 035120 (2011).
24. Chiu, C. K., Vazifeh, M. M. & Franz, M. Majorana fermion exchange in strictly one dimensional structures. *arXiv* 1403.0033 (2014).
25. Alicea, J. *et al.* Non-Abelian statistics and topological quantum information processing in 1D wire networks. *Nat. Phys.* **7**, 412–417 (2011).
26. Sau, J. D., Clarke, D. J. & Tewari, S. Majorana fermions in chiral topological ferromagnetic nanowires. *Phys. Rev. B* **84**, 094505 (2011).
27. Heck, B. *et al.* Coulomb-assisted braiding of Majorana fermions in a Josephson junction array. *New J. Phys.* **14**, 035019 (2012).
28. Kraus, C. V., Zoller, P. & Baranov, M. A. Braiding of atomic Majorana fermions in wire networks and implementation of the Deutsch-Jozsa algorithm. *Phys. Rev. Lett.* **111**, 203001 (2013).
29. Laflamme, C., Baranov, M. A., Zoller, P. & Kraus, C. V. Hybrid topological quantum computation with Majorana fermions: A cold-atom setup. *Phys. Rev. A* **89**, 022319 (2014).
30. Oka, T. & Aoki, H. Photovoltaic Hall effect in graphene. *Phys. Rev. B* **79**, 081406 (2009).
31. Kitagawa, T., Berg, E., Rudner, M. & Demler, E., Topological characterization of periodically driven quantum systems. *Phys. Rev. B* **82**, 235114 (2010).
32. Lindner, N. H., Refael, G. & Galitski, V. Floquet topological insulator in semiconductor quantum wells. *Nat. Phys.* **7**, 490 (2011).
33. Gu, Z., Fertig, H. A., Arovas, D. P. & Auerbach, A. Floquet spectrum and transport through an irradiated graphene ribbon. *Phys. Rev. Lett.* **107**, 216601 (2011).
34. Jiang, L. *et al.* Majorana fermions in equilibrium and in driven cold-atom quantum wires. *Phys. Rev. Lett.* **106**, 220402 (2011).
35. Liu, D. E., Levchenko, A. & Baranger, H. U. Floquet Majorana fermions for topological qubits in superconducting devices and cold-atom systems. *Phys. Rev. Lett.* **111**, 047002 (2013).
36. Katan, Y. T. & Podolsky, D. Modulated Floquet topological insulators. *Phys. Rev. Lett.* **110**, 016802 (2013).
37. Rudner, M. S., Lindner, N. H., Berg, E. & Levin, M. Anomalous edge states and the bulk-edge correspondence for periodically driven two-dimensional systems. *Phys. Rev. X* **3**, 031005 (2013).
38. Foa Torres, L. E. F., Perez-Piskunow, P. M., Balseiro, C. A. & Usaj, G. Multiterminal conductance of a floquet topological insulator. *Phys. Rev. Lett.* **113**, 266801 (2014).
39. Benito, M. *et al.* Floquet engineering of long-range p -wave superconductivity. *Phys. Rev. B* **90**, 205127 (2014).
40. Lababidi, M., Satija, I. I. & Zhao, E. Counter-propagating edge modes and topological phases of a kicked quantum Hall system. *Phys. Rev. Lett.* **112**, 026805 (2014).

41. Perez-Piskunow, P. M., Usaj, G., Balseiro, C. A. & Foa Torres, L. E. F. Floquet chiral edge states in graphene. *Phys. Rev. B* **89**, 121401 (2014).
42. Li, Y., Kundu, A., Zhong, F. & Seradjeh, B. Tunable Floquet Majorana fermions in driven coupled quantum dots. *Phys. Rev. B* **90**, 121401 (2014).
43. Xue, Z. Y. *et al.* Robust interface between flying and topological qubits. *Sci. Rep.* **5**, 12233 (2015).
44. Alicea, J. Majorana fermions in a tunable semiconductor device. *Phys. Rev. B* **81**, 125318 (2010).
45. Stoudenmire, E. M., Alicea, J., Strykh, O. A. & Fisher, M. P. A. Interaction effects in topological superconducting wires supporting Majorana fermions. *Phys. Rev. B* **84**, 014503 (2011).
46. Flensberg, K. Non-Abelian operations on Majorana fermions via single-charge control. *Phys. Rev. Lett.* **106**, 090503 (2011).
47. Budich, J. C., Walter, S. & Trauzettel, B. Failure of protection of Majorana based qubits against decoherence. *Phys. Rev. B* **85**, 121405 (2012).
48. Goldstein, G. & Chamon, C. Decay rates for topological memories encoded with Majorana fermions. *Phys. Rev. B* **84**, 205109 (2011).
49. Rainis, D. & Loss, D. Majorana qubit decoherence by quasiparticle poisoning. *Phys. Rev. B* **85**, 174533 (2012).
50. Mazza, L., Rizzi, M., Lukin, M. D. & Cirac, J. I. Robustness of quantum memories based on Majorana zero modes. *Phys. Rev. B* **88**, 205142 (2013).
51. Karzig, T., Pientka, F., Refael, G. & Oppen, F. Shortcuts to non-Abelian braiding. *Phys. Rev. B* **91**, 201102 (2015).
52. Creffield, C. E. & Platero, G. Dynamical control of correlated states in a square quantum dot. *Phys. Rev. B* **66**, 235303 (2002).
53. Creffield, C. E. Location of crossings in the Floquet spectrum of a driven two-level system. *Phys. Rev. B* **67**, 165301 (2003).
54. Silveri, M. P. *et al.* Stückelberg interference in a superconducting qubit under periodic latching modulation. *New J. Phys.* **17** 043058 (2015).
55. Leijnse, M. & Flensberg, K. Hybrid topological-spin qubit systems for two-qubit-spin gates. *Phys. Rev. B* **86**, 104511 (2012).
56. Leijnse, M. & Flensberg, K. Quantum information transfer between topological and spin qubit systems. *Phys. Rev. Lett.* **107**, 210502 (2011).
57. Bravyi, S. Universal quantum computation with the $\nu = 5/2$ fractional quantum Hall state. *Phys. Rev. A* **73**, 042313 (2006).
58. Deng, M. T. *et al.* Anomalous zero-bias conductance peak in a Nb-InSb Nanowire-Nb hybrid device. *Nano Lett.* **12**, 6414 (2012).
59. Finck, A. D. K. *et al.* Anomalous modulation of a zero-bias peak in a hybrid nanowire-superconductor device. *Phys. Rev. Lett.* **110**, 126406 (2013).
60. Petta, J. R. *et al.* Manipulation of a single charge in a double quantum dot. *Phys. Rev. Lett.* **93**, 186802 (2004).
61. Pettersson, K. D., Petta, J. R., Lu, H. & Gossard, A. C. Quantum coherence in a one-electron semiconductor charge qubit. *Phys. Rev. Lett.* **105**, 246804 (2010).
62. Nadj-Perge, S., Frolov, S. M., Bakkers, E. P. A. M. & Kouwenhoven, L. P. Spin-orbit qubit in a semiconductor nanowire. *Nature* **468**, 1084 (2010).
63. Shirley, J. H. Solution of the Schrodinger equation with a Hamiltonian periodic in time. *Phys. Rev.* **138**, B979 (1965).
64. Sambe, H. Steady states and quasienergies of a quantum-mechanical system in an oscillating field. *Phys. Rev. A* **7**, 2203 (1973).
65. Holthaus, M. The quantum theory of an ideal superlattice responding to far-infrared laser radiation. *Z. Phys. B: Condens. Matter* **89**, 251 (1992).
66. Creffield, C. E. & Platero, G. ac-driven localization in a two-electron quantum dot molecule. *Phys. Rev. B* **65**, 113304 (2002).

Acknowledgements

We thank S. M. Frolov for helpful discussions. This work is supported by the National Natural Science Foundation of China (Grants No. 11534002 and No. 61475033).

Author Contributions

X.X.Y. proposed the idea and led the study, Z.C.S. and X.X.Y. performed the analytical and numerical calculations, Z.C.S., W.W. and X.X.Y. prepared the manuscript, all authors reviewed the manuscript.

Additional Information

Competing financial interests: The authors declare no competing financial interests.

How to cite this article: Shi, Z. C. *et al.* Quantum gates by periodic driving. *Sci. Rep.* **6**, 22077; doi: 10.1038/srep22077 (2016).



This work is licensed under a Creative Commons Attribution 4.0 International License. The images or other third party material in this article are included in the article's Creative Commons license, unless indicated otherwise in the credit line; if the material is not included under the Creative Commons license, users will need to obtain permission from the license holder to reproduce the material. To view a copy of this license, visit <http://creativecommons.org/licenses/by/4.0/>